PROCEEDINGS OF SCIENCE

Simulations of the Yield Functions of a Semi-Leaded Neutron Monitor from Latitude Surveys.

A. Seripienlert,[a,*] **W. Nuntiyakul,**[b] **S. Khamphakdee,**[b] **P.-S. Mangeard,**[c] **A. Pagwhan,**[d,b] **A. Sáiz,**[d] **D. Ruffolo,**[d] **P. Evenson,**[c] **K. Fongsamut,**[b] **P. Jiang,**[e] **P. Chuanraksasat,**[a] **K. Munakata,**[f] **J. Madsen,**[g] **B. Soonthornthum**[a] **and S. Komonjinda**[b]

[a] *National Astronomical Research Institute of Thailand (NARIT), Chiang Mai 50180, Thailand*
[b] *Department of Physics and Materials Science, Faculty of Science, Chiang Mai University, Chiang Mai 50200, Thailand*
[c] *Department of Physics and Astronomy, University of Delaware, Newark, DE 19716, USA*
[d] *Department of Physics, Faculty of Science, Mahidol University, Bangkok 10400, Thailand*
[e] *Polar Research Institute of China, Pudong, Shanghai 200136, China*
[f] *Physics Department, Shinshu University, Matsumoto, Nagano 390-8621, Japan*
[g] *Wisconsin IceCube Particle Astrophysics Center, University of Wisconsin-Madison, WI 53703, USA*

E-mail: achara@narit.or.th

Cosmic rays are highly energetic particles from space. When cosmic rays hit the Earth's atmosphere, they produce a cascade of subatomic particles. A large portion of these particles are neutrons which can be detected using a neutron monitor either at a fixed location or shipborne. Shipborne neutron monitors have an advantage in that they can measure particles over a wide range of rigidity by conducting a latitude survey. In Thailand, we assembled the Changvan neutron monitor, a mobile NM64-type monitor consisting of three units of 10BF3 gas-filled proportional counters – only two of which are surrounded by lead. We made two expeditions (2018 and 2019 survey years) by sailing the Changvan from Shanghai to Antarctica and back. To study the energy-dependent effective area (yield function) of the Changvan leaded and unleaded counters, we perform a Monte-Carlo simulation in two steps. The first step simulates the interaction of the cosmic rays in the atmosphere and records the secondary particles that reach sea level. The second step injects these particles into a model of the detector with surroundings. Multiple atmospheric profiles are used to probe how changes affect the differential response function (DRF). We compare the simulated DRF with data taken during the survey year 2019. We investigate and discuss the differences in the DRF between the two leaded edge counters and the unleaded middle counter, all of which are inside the same reflector.

38th International Cosmic Ray Conference (ICRC2023)
26 July - 3 August, 2023
Nagoya, Japan

ICRC2023
38th International Cosmic Ray Conference
The Astroparticle Physics Conference

*Speaker

PoS(ICRC2023)1334

1. Introduction

A neutron monitor (NM) is a detector, either ground-based or sea-based, used for measuring the flux of high-energy cosmic ray neutrons. The standard neutron monitor, known as NM64, was developed by Hatton and Carmichael in 1964 [1]. NMs typically employ highly efficient neutron-detecting gases, such as boron-10 and helium-3. When cosmic ray neutrons interact with these gases, they produce detectable signals. The NM64 consists of four essential components: i) an outermost polyethylene reflector, ii) lead rings for generating lower energy neutrons to amplify the signal, iii) a moderator made of high-density polyethylene to slow down the neutrons, and iv) The innermost component of the NM64 is a proportional counter filled with either BF_3 gas enriched to 96% of the ^{10}B isotope or He_3 enriched with 97% helium-3 and 3% CO_2. NMs play a crucial role in studying cosmic rays and their effects on Earth's atmosphere and space weather. They are used to monitor fluctuations in cosmic ray flux over time, providing valuable information about solar activity, geomagnetic disturbances, and potential health hazards for astronauts and aviation crew members at high altitudes.

In this work, we use data obtained from the "Changvan" neutron monitor, a portable monitor employed to measure neutron flux during round trips between Shanghai, China, and the Antarctic over a span of two survey years. This experiment is commonly known as a "latitude survey," where the neutron monitor (NM) is rapidly transported through a range of cutoff rigidities (momentum per unit charge) [2]. By observing the variation in the NM's counting rate with respect to cutoff rigidity, we can measure the cosmic ray spectrum (averaged over particle type) typically at higher energies than direct spacecraft measurements [3–6]. The Changvan consists of three neutron-sensitive proportional counters assembled according to the standard NM64 design, with the exception that the middle counter lacks the lead producer. We refer to this modified design as a "semi-leaded neutron monitor" [7–10]. The Changvan incorporates BF_3 gas to induce nuclear fission through the reaction ^{10}B (n, α)^{7}Li. Consequently, ionization bursts occur, generating electrical pulses on a wire maintained at a potential of approximately -2,800 V. An electronic module counts these electric pulses and transmits the data to the data acquisition system. Conducting latitude surveys with NMs offers the advantage of determining the energy-dependent effective area (yield function) at sea level through direct measurements [6]. In our approach, we use the Earth as a magnetic spectrometer, and we employ Monte-Carlo simulations as a tool to investigate the yield function at the detector's altitude. The aim of this study is to validate the accuracy of Monte Carlo simulations using three atmospheric models of Hobart, Shanghai, and Zhonshang, in preparation for acquiring a precise yield function.

2. Data Observation

In this work, we used data from the 2019 survey conducted by Changvan. The Changvan was deployed on the icebreaking vessel Xuelong during its journey from Shanghai to Zhongshan station in Antarctica for two survey years. Specifically, we focused on data from the second survey, which took place from October 21, 2019, to April 22, 2020. Figure 1 shows the route of the Changvan monitor during the 2019 survey year. We used the count rate data provided in [8] for the southbound data in 2019. Additionally, we obtained supplementary data from the same survey year from [9].

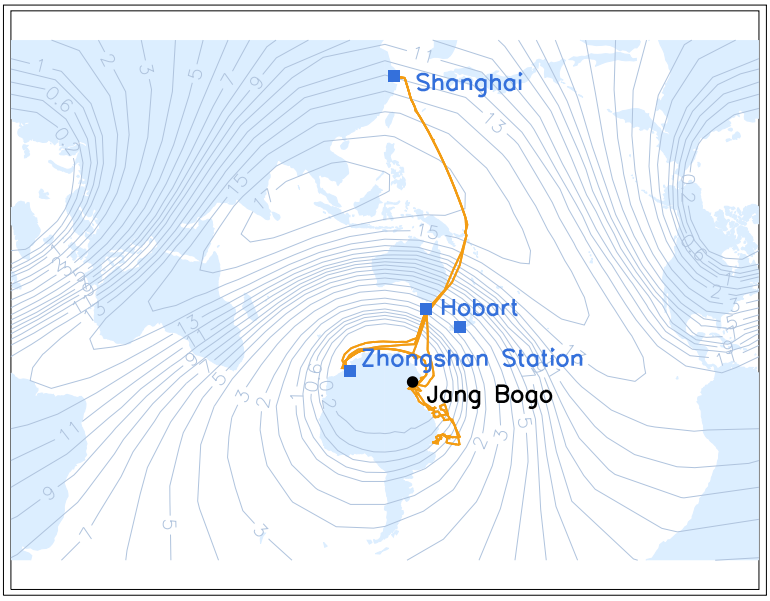

Figure 1: Path of Changvan in the 2019 survey year (orange line). The contour lines accompanied by numerical values represent the vertical cutoff rigidity, expressed in units of GV, calculated for February 11, 2019, at 12:00 UT.

We conducted data reduction and correction procedures for the semi-leaded Changvan monitor data. This included applying a conventional neutron monitor correction method and rectifying the pressure data, as described in [4]. We used the correction equation $\beta = 1.006\times10^{-2} - 1.53\times10^{-4}P_c$ %/mmHg, with a reference pressure P_{ref} of 760 mmHg, representing sea level pressure.

We observed a significant decrease in count rates from November 21-24, 2019, when the ship was docked at Zhongshan station for cargo loading. This decrease was attributed to the instrument being covered by other cargo containers during unloading. To ensure the use of uncontaminated data, we excluded the affected data from further analysis. Despite removing the affected data, there remained a noticeable discontinuity in the count rate. We concluded that this shift occurred due to changes in the ship's configuration. During the 2019 survey year, the ship was heavily loaded on its journey to Antarctica but empty on its return to Shanghai. The Changvan was transported with other containers on an open deck, rather than separately. This indicates that the presence of other containers significantly affected the yield function of the Changvan during the southbound segment. Therefore, we did not use the southbound segment for this study.

3. Simulations

3.1 Atmospheric Simulations

In this work, we use FLUKA (FLUktuierende KAskade), version 4.1-1, which is an open-source particle physics package available at `https://fluka.cern/` [11, 12]. The hadron interaction models of DPMJET were employed [13, 14]. The simulation process consists of two parts: i) Atmospheric simulation and ii) Detector simulation. After obtaining outputs from FLUKA, we analyzed the simulated integral and differential response functions, as well as count rates.

The Atmospheric simulation involved creating an atmospheric profile using data from the Global Data Assimilation System (GDAS) for pressure surfaces ranging from 20 to 1000 hPa and the Naval Research Laboratory Mass Spectrometer, Incoherent Scatter Radar Extended model

Type	No. of simulated particles								
	Rigidity 1-10 GV			Rigidity 10-200 GV			Rigidity 200-500 GV		
	Hob	Sha	Zho	Hob	Sha	Zho	Hob	Sha	Zho
	Atmospheric simulations								
p	10M	10M	10M	1M	1M	1M	1M	1M	1M
α	10M	10M	10M	1M	1M	1M	1M	1M	1M
	Library								
n	104441	93771	120957	136508	125494	155272	925016	853698	1029597
p	5163	4523	5955	13486	12147	15443	109524	99484	122149
$\mu^{\pm}$	16592	15304	18988	1149070	1126119	1200135	14247188	14023234	14697068
	Detector simulations								
n	1000M	1000M	1000M	100M	100M	100M	100M	100M	100M
p	1000M	1000M	1000M	100M	100M	100M	100M	100M	100M
$\mu^{\pm}$	1000M	720M	743.5M	100M	100M	100M	88.5M	51M	51.5M

Table 1: FLUKA simulation statistics: M denotes one million particles.

(NRLMSISE-00) for higher altitudes [15]. A spherical atmosphere was assumed, following the methodology described in [16]. Generated atmospheric profiles of Shanghai, Hobart, and Zhongshan were used. Isotropic primary particles with rigidity ranging from 1 GV to 500 GV were simulated. These particles were divided into three intervals (1-10 GV, 10-200 GV, and 200-500 GV) with different statistics, as shown in Table 1.

3.2 Detector Simulations

The Detector simulation employed the detector geometry created using Flair 3.1 [17], as shown in Figure 1 in [10]. A geometric model of Changvan mounted on the Xuelong icebreaker positioned above seawater beneath the ship's lower half-spherical geometry. Secondary particles from the libraries were randomly selected and uniformly injected above the detector. The statistical runs for neutrons (n), protons (p), and muons ($\mu^{\pm}$) are specified in Table 1. A dead time of 20 μs was applied, which was the same for all three tubes. We incorporated the modulation parameter ϕ = 426 MV, as determined by Usoskin et al. in 2017 [18, 19], into our simulations.

The simulated count rates were corrected for pressure using the pressure coefficient (β) as a function of cutoff rigidity (P_c), as explained in section 2. Barometric pressures of 756.8 mmHg, 766.5 mmHg, and 745.7 mmHg were applied to the atmospheric models at Hobart, Shanghai, and Zhongshan, respectively. The reference pressure (P_{ref}) was defined as 760 mmHg.

4. Integral and Differential Response Functions

The neutron monitor records the hadronic component within atmospheric secondary radiation from primary cosmic rays continuously. The count of these secondary particles is connected to the primary spectrum above the atmosphere through the atmospheric yield function. Simpson (1948) [20] observed that the latitude variation of the secondary hadronic component was considerably larger than that of the muon component, indicating the neutron monitor's heightened sensitivity to lower energies in the primary spectrum [21].

Figure 2 illustrates the relationship between the number of counts (N) and the geomagnetic cutoff rigidity (P_c). The left panels display the integral response function. The actual and simulated

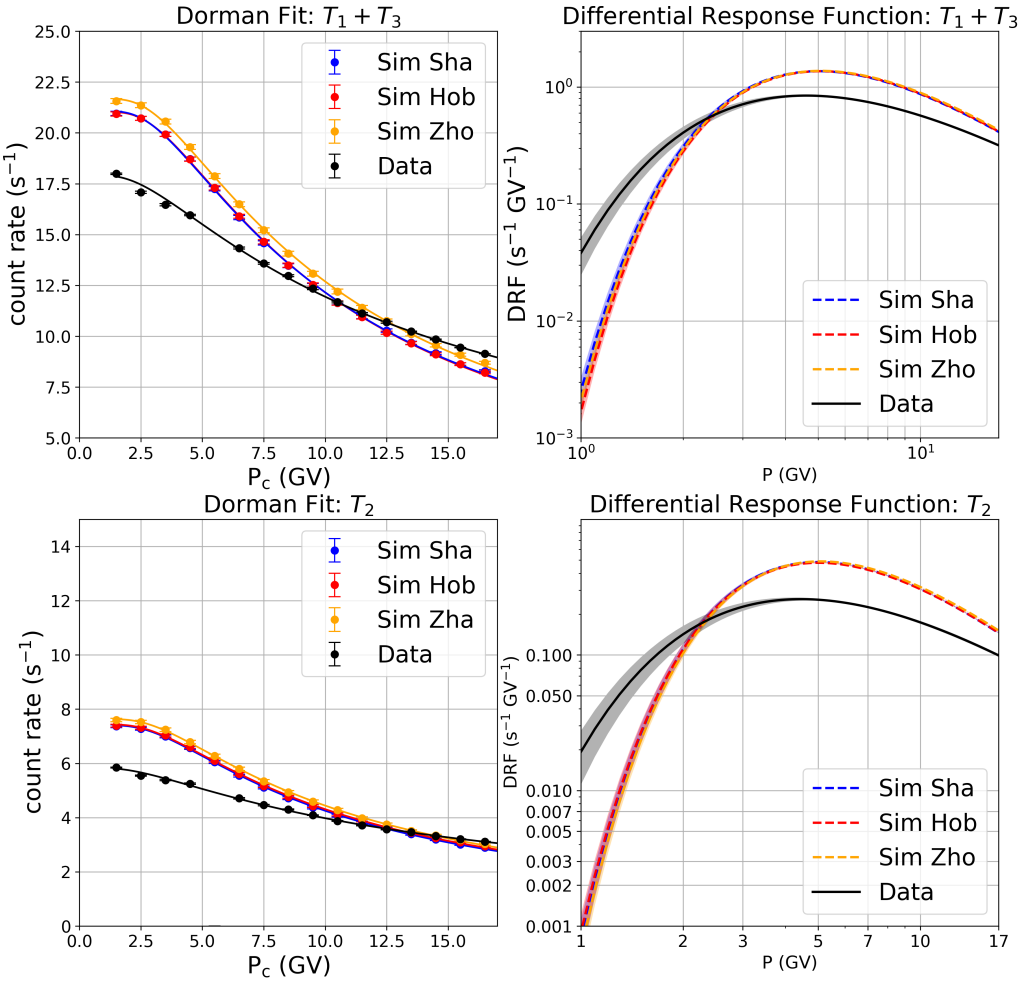

Figure 2: The response functions for simulations at three atmospheric models (Shanghai (Sha), Hobart (Hob), and Zhongshan (Zho)) and for the data are displayed. The left panels show the integral response functions, while the right panels show the differential response functions derived from the Dorman function. The upper panels correspond to the leaded tubes from the edge tubes of T_1 and T_3, while the lower panels correspond to the unleaded tube of the middle tube of T_2.

count rates are plotted as averages at the center cutoff rigidity bin (1.5, 2.5, 3.5, ..., 16.5 GV). We performed a fitting analysis of the data to the Dorman function [22] given by Eq. (1), where N_0, α, and κ are free parameters. The fit covers the range from 1.5 GV to 16.5 GV. Next, we used the parameter values obtained and applied them to Eq. (2). This yielded the Dorman fit, which is shown in the right panels of Figure 2. The upper panels showcase the response functions of the combined leaded side tubes (T_1+T_3), while the lower panels display those of the unleaded tube (T_2). Error bands in differential response functions represent 1σ statistical uncertainty.

$$N = N_0(1 - e^{-\alpha P^{-\kappa} c}), \quad (1)$$

$$DRF = N_0 \alpha P^{-\kappa-1} \kappa (e^{-\alpha P^{-\kappa}}). \quad (2)$$

5. Results and Conclusions

In Figure 2, after correcting the simulated count rates for pressure at sea level, we observe their similarity across three atmospheric models. Comparing simulation and data results, the rigidity responses of both leaded (T_1+T_3) and unleaded (T_2) detectors show greater consistency at higher cutoff rigidity (> 10 GV) than at lower cutoff rigidity.

To further investigate, we plotted Figure 3, which shows the ratios of DRF for leaded (left panel) and unleaded (right panel) detectors relative to different atmospheres (Hobart/Shanghai and Hobart/Zhongshan) against geomagnetic cutoff, P_c.

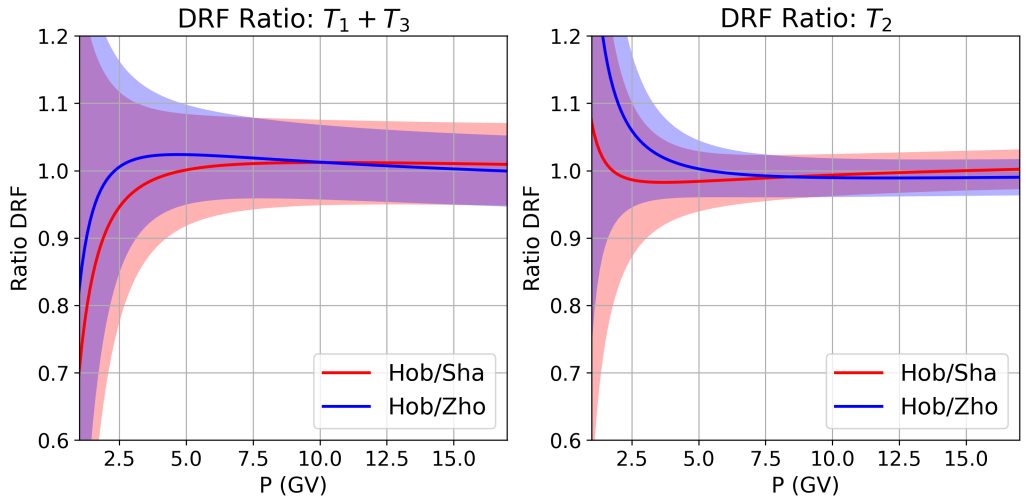

Figure 3: The ratios of the differential response function (DRF), normalized $N_0 = 1$, were examined between the different atmospheric models.

In the data analysis, a clear trend emerges: the leaded/unleaded count rate ratio consistently decreases as P_c increases, as depicted in Figure 4 (left panel). This finding suggests that the unleaded detector exhibits a stronger rigidity response compared to the leaded detector at higher P_c. However, the simulation results deviate from this trend by approximately 10% at low cutoff rigidity and about 4% at higher cutoff rigidity. The $\pm 1\sigma$ error bars complicate the identification of discernible trends in the simulated count rate ratios across the three atmospheric models.

Our analysis includes the examination of the count rate leaded/unleaded ratios of DRF with a normalization factor of $N_0 = 1$, covering both simulated and actual data. As shown in Figure 4 (right panel), we present an example illustrating the leaded/unleaded ratio plotted against (P_c) in the Hobart atmosphere.

In summary, this study reveals that our normalized simulated differential response function closely matches the real data within ±10%. However, the observed ratio does not exhibit a clear proportional trend at higher geomagnetic cutoffs, in contrast to the findings from the real data.

6. Acknowledgments

This work was supported by NARIT, Chiang Mai University (CMU), the NSRF via the Program Management Unit for Human Resources & Institutional Development, Research, and Innovation

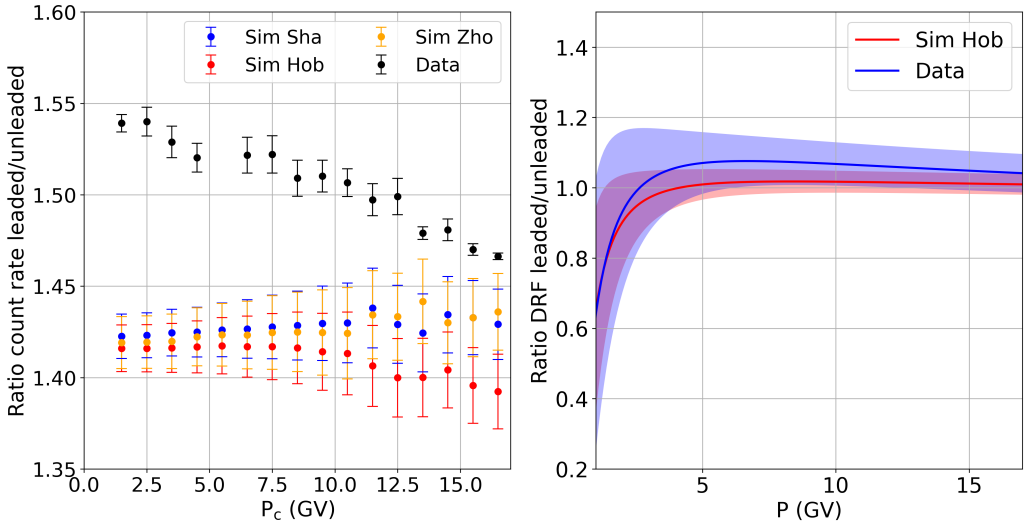

Figure 4: (Left) The ratios of the leaded to unleaded detectors, represented as $(T_1+T_3)/T_2$, were obtained as a function of cutoff rigidity (P_c). These ratios were derived from both the data and simulations for the three atmospheric models at Shanghai, Zhongshan, and Hobart. (Right) The ratios of the differential response function (DRF), normalized $N_0 = 1$, were examined between the leaded to unleaded as well as between the simulations and data.

[grant number B39G660028], and NSTDA and NRCT under the High-Potential Research Team Grant Program (N42A650868). We thank the Center for Information Technology (CIT) team of NARIT and ITSC of CMU for providing server on-demand for simulations. We would also like to extend our appreciation to the Northern Science Park (Chiang Mai) for providing laboratory space that facilitated the smooth functioning of our research team.

References

[1] C.J. Hatton and H. Carmichael, *Experimental Investigation of the NM-64 Neutron Monitor*, *Can. J. Phys.* **42** (1964) 2443.

[2] J.M. Clem, J.W. Bieber, P. Evenson, D. Hall, J.E. Humble and M. Duldig, *Contribution of obliquely incident particles to neutron monitor counting rate*, *J. Geophys. Res.* **102** (1997) 26919.

[3] J.W. Bieber, J.M. Clem, M.L. Duldig, P.A. Evenson, J.E. Humble and R. Pyle, *Latitude survey observations of neutron monitor multiplicity*, *J. Geophys. Res. Space Phys.* **109** (2004) A12106.

[4] W. Nuntiyakul, P. Evenson, D. Ruffolo, A. Sáiz, J.W. Bieber, J. Clem et al., *Latitude Survey Investigation of Galactic Cosmic Ray Solar Modulation during 1994-2007*, *Astrophys. J.* **795** (2014) 11.

[5] W. Nuntiyakul, A. Sáiz, D. Ruffolo, P.S. Mangeard, P. Evenson, J.W. Bieber et al., *Bare Neutron Counter and Neutron Monitor Response to Cosmic Rays During a 1995 Latitude Survey*, *J. Geophys. Res. Space Phys.* **123** (2018) 7181.

[6] W. Nuntiyakul, P.S. Mangeard, D. Ruffolo, P. Evenson, J.W. Bieber, J. Clem et al., *Direct*

Determination of a Bare Neutron Counter Yield Function, *J. Geophys. Res. Space Phys.* **125** (2020) e27304.

[7] K. Fongsamut, P. Jiang, W. Nuntiyakul, A. Sáiz, D. Ruffolo, P.S. Mangeard et al., *Preliminary FLUKA simulations of the Changvan Neutron Monitor*, in *J. Phys.: Conf. Ser.*, vol. 1719, p. 012004, Jan., 2021, DOI.

[8] S. Khamphakdee, P. Jiang, P. Chuanraksasat, W. Nuntiyakul, D. Ruffolo, A. Sáiz et al., *Preliminary analysis of the Changvan neutron monitor operation in latitude surveys during 2019-2020*, in *J. Phys.: Conf. Ser.*, vol. 1719, p. 012010, Jan., 2021, DOI.

[9] P. Yakum, P. Jiang, P. Chuanraksasat, W. Nuntiyakul, D. Ruffolo, A. Sáiz et al., *Preliminary analysis of neutron time-delay histograms from Changvan latitude surveys*, in *J. Phys.: Conf. Ser.*, vol. 1719, p. 012006, Jan., 2021, DOI.

[10] A. Seripienlert, W. Nuntiyakul, S. Khamphakdee, P.S. Mangeard, A. Sáiz, D. Ruffolo et al., *Validation of Monte Carlo Yield Function of a Semi-Leaded Neutron Monitor using Latitude Survey Data in 2019 and 2020*, in *37th ICRC*, p. 1243, Mar., 2022, DOI.

[11] G. Battistoni, T. Boehlen, F. Cerutti, P.W. Chin, L.S. Esposito, A. Fassò et al., *Overview of the fluka code*, *Ann. Nucl. Energy* **82** (2015) 10.

[12] C. Ahdida, D. Bozzato, D. Calzolari, F. Cerutti, N. Charitonidis, A. Cimmino et al., *New capabilities of the fluka multi-purpose code*, *Front. Phys* **9** (2022) .

[13] S. Roesler, R. Engel and J. Ranft, *The monte carlo event generator dpmjet-iii*, in *Advanced Monte Carlo for Radiation Physics, Particle Transport Simulation and Applications*, A. Kling, F.J.C. Baräo, M. Nakagawa, L. Távora and P. Vaz, eds., (Berlin, Heidelberg), pp. 1033–1038, Springer Berlin Heidelberg, 2001.

[14] A. Fedynitch, *Cascade equations and hadronic interactions at very high energies*, Ph.D. thesis, KIT, Karlsruhe, Dept. Phys., 2015.

[15] J.M. Picone, A.E. Hedin, D.P. Drob and A.C. Aikin, *NRLMSISE-00 empirical model of the atmosphere: Statistical comparisons and scientific issues*, *J. Geophys. Res. Space Phys.* **107** (2002) 1468.

[16] P.S. Mangeard, D. Ruffolo, A. Sáiz, S. Madlee and T. Nutaro, *Monte Carlo simulation of the neutron monitor yield function*, *J. Geophys. Res. Space Phys.* **121** (2016) 7435.

[17] V. Vlachoudis, *Flair: A powerful but user friendly graphical interface for fluka*, in *Proc. Int. Conf. on Mathematics, Computational Method & Reactor Physics*, 04, 2009.

[18] I.G. Usoskin, A. Gil, G.A. Kovaltsov, A.L. Mishev and V.V. Mikhailov, *Heliospheric modulation of cosmic rays during the neutron monitor era: Calibration using PAMELA data for 2006-2010*, *J. Geophys. Res. Space Phys.* **122** (2017) 3875 [1705.07197].

[19] E.E. Vos and M.S. Potgieter, *New Modeling of Galactic Proton Modulation during the Minimum of Solar Cycle 23/24*, *Astrophys. J.* **815** (2015) 119.

[20] J.A. Simpson, *The Latitude Dependence of Neutron Densities in the Atmosphere as a Function of Altitude*, *Phys. Rev.* **73** (1948) 1389.

[21] J.M. Clem and L.I. Dorman, *Neutron Monitor Response Functions*, *Space Sci. Rev.* **93** (2000) 335.

[22] L.I. Dorman, *Barometer effect of cosmic rays and changes of the energy spectrum and cut-off rigidities. The method of the partial barometer coefficients*, in *ICRC*, vol. 2 of *ICRC*, p. 715, Jan., 1970.